Original Research Article: full paper

(2022), «EUREKA: Physics and Engineering»
Number 4

STUDY OF THE SECONDARY CHARACTERISTICS OF THE BISTATIC SCATTERING OF A COMBINED OBJECT IN A COVERT RADAR SURVEILLANCE SYSTEM

Stanislav Horielyshev
Scientific and Research Center of Service and Military Activities of the National Guard of Ukraine[1]

Pavlo Volkov
Adjunct Doctoral and Adjunct [1]

Igor Boikov✉
Department of Armoured Vehicles[1]
biv543@ukr.net

Dmitro Baulin
Scientific and Research Center of Service and Military Activities of the National Guard of Ukraine[1]

Hryhorii Ivanets
Department of Fire Tactics and Rescue Operations
National University of Civil Defence of Ukraine
94 Chernyshevska str., Kharkiv, Ukraine, 61023

Aleksandr Nakonechnyi
Department of Armament of Air Defense of Ground Forces
Ivan Kozhedub Kharkiv National Air Force University
77/79 Symska str., Kharkiv, Ukraine, 61023

Svyatoslav Manzhura
Scientific and Research Center of Service and Military Activities of the National Guard of Ukraine[1]

Valentyn Yuriev
Faculty of Postgraduate Education
Kharkiv National University of Radio Electronics
14 Nauky ave., Kharkiv, Ukraine, 61166

Natalia Gleizer
Department of Physics
H. S. Skovoroda Kharkiv National Pedagogical University
2 Valentynivska str., Kharkiv, Ukraine, 61168

[1]*National Academy of the National Guard of Ukraine*
3 Zakhysnykiv Ukrainy sq., Kharkiv, Ukraine, 61001

✉**Corresponding author**

Abstract

The emergence of new means of attack, reconnaissance and methods of sabotage imposes special requirements on the technical means of protecting important state facilities (ISF). Modern trends in the construction of ISF physical protection systems are the integration of engineering barriers, perimeter signaling and detection tools. Detection tools should provide covert receipt of information about the approach of the intruder in «distant» intrigues. To do this, it is possible to use technical means built on the principle of semi-active bistatic radar with an external illumination source. However, in order to identify intruders in the ISF protection zone, it is necessary to have a priori information about the radar visibility of the combined location objects. The combined object is typically a complex object having both metallic and dielectric elements.

To this end, a technique has been developed for estimating the radar cross-section (RCS) of combined objects in the field of external illumination. The electromagnetic field (EMF) scattered by a combined object in the meter and decimeter wavelength

ranges is calculated as a coherent sum of fields, taking into account their phase, scattered by its metal and dielectric elements. This made it possible to take into account the electromagnetic interaction of the elements of the combined object. The method of integral equations (IE) was used to find the current density and magnetic field strength.

The scatter diagrams of the person-intruder, the person-intruder in personal armor protection (PAP) under different conditions of irradiation and reception and illumination frequencies are obtained and analyzed. This made it possible to evaluate the effect of metallic elements on the scatter diagram of the combined object.

The obtained a priori information is of significant practical importance at the stage of optimizing signal processing algorithms and designing new means of covert detection.

Keywords: covert surveillance system, effective scattering surface, combined object, integral equations, illumination source.

DOI: 10.21303/2461-4262.2022.002493

1. Introduction

In modern conditions, the growth of political instability in the world, the exacerbation of migration processes, the issues of ensuring the security of sections of the borders of countries and the ISF are becoming relevant. Of particular danger are the criminal unauthorized actions of illegal armed formations or individual intruders: terrorists, saboteurs, extremists [1, 2]. The emergence of new means of attack, reconnaissance and methods of sabotage imposes special requirements on the technical means of protecting objects. This is the secrecy of work, the identification of intruders at long distances and in all weather conditions.

Modern trends in the construction of protected systems for the physical protection of objects is the integration of engineering barriers, perimeter signaling and detection tools. Detection tools should provide covert receipt of information about the approach of the intruder to the ISF in «distant» intrigues [3]. As such technical means, it is possible to use technical means built on the principle of semi-active bistatic radar with an external illumination source. In space, there are a lot of radio signals for various purposes: radio broadcasting, cellular communications, television, satellite navigation signals, signals of radio relay lines, etc. In [4], consider the features of the above signals, their main parameters (bandwidth, duration, spectrum width, power, frequency range) and the possibility of using them to obtain radar information in semi-active radar stations. It has been established that the most promising are terrestrial transmitters with a T2 digital television signal (up to 800 MHz), space transmitters with a digital signal (1–3 GHz), and a cellular communication system transmitter (GSM-900, GSM-1800).

The issues of building semi-active bistatic radars (NBRLS) with external illumination signals are given great attention in such countries [5]:

– USA (NBRLS «Silent Sentry» manufactured by «Lockheed-Martin», specialized passive multistatic radar «Manastash Ridge Radar» manufactured by the University of Washington);

– Great Britain (NBRLS «Celldar» manufactured by «Roke Manor»);

– France (radar system for detecting low-flying targets «Homeland Alerter 100», «Sinbad» manufactured by «Thales»);

– Italy (passive hidden radar PCR «Aulos» manufactured by «Selex ES»);

– Germany (mobile experimental NBRLS «Cora» developed by Fraunhofer FHR);

– Poland (family of experimental NBRLS «PaRaDe» developed by the Warsaw University of Technology);

– The Netherlands, Norway, South Africa, China, Iran and others.

In these countries, existing industrial designs or experimental mock-ups have been created.

However, in order to detect any radar objects (for example, intruders in the ISF protection zone), it is necessary to have a priori information about their radar visibility under various conditions.

The intruder person in the study is considered as a dielectric object with the electrophysical properties of biological tissues. The intruder person in the PAP as a combined object. In the general case, a combined object is an object of complex shape, containing elements of different electrical sizes and shapes with different electrodynamic characteristics. In this study, under the combined object, let's consider an object that includes both metal and dielectric elements. The RCS of such an object consists of scattered EMF of individual metal and dielectric elements and their electromagnetic interaction, which greatly complicates the solution of this problem.

Therefore, obtaining and analyzing the secondary scattering characteristics (SSC), in particular the RCS, of such objects is an urgent scientific and practical problem. The solution of this problem will make it possible to substantiate the requirements for a system of covert surveillance of the area of responsibility and improve the signal processing algorithms for detecting these objects.

To obtain the RCS values of different objects, including combined ones, both methods of physical [6, 7] and mathematical modeling are used. The advantages of physical modeling are visibility, the ability to study processes in real conditions. However, physical modeling requires significant financial, time and material costs, depending on the nature of the experiment, the availability of verified metrological equipment. The use of mathematical modeling methods has a number of advantages over physical modeling. For example, a variety of radar sounding scenarios that can be simulated in a relatively short time, no additional costs for calculations, and others. At the same time, more stringent requirements are imposed on mathematical methods in terms of the accuracy of reproducing the scattering characteristics of radar objects.

At present, a large number of works have been published in which the theoretical foundations are outlined and the numerical implementation of methods for calculating the RCS of various types of radar objects is proposed.

There are no universal methods suiTable for modeling SSC of complex objects. The choice of modeling method depends on the electrical dimensions of the object relative to the wavelength, its complexity and the materials from which its elements are made.

The well-known asymptotic high-frequency methods (AHFM) of calculation include methods of geometric optics (GO) [8, 9], geometric theory of diffraction (GTD) [10, 11], physical optics (PO) [9, 10, 12], physical theory of diffraction (PTD) [8, 10, 13]. All AHFMs are based on strict representations of electromagnetic fields and can be obtained from them under certain assumptions about the object. The advantages of these methods are simplicity in computer implementation, high accuracy and speed of calculations. Among the shortcomings, one can note the presence of application limits, in particular, only for objects with geometric dimensions of scatterers exceeding the wavelength by tens of percent. For this study, where the dimensions of objects in the wavelength range of T2 TV transmitters or cellular communications are comparable to the wavelength (resonant), AHFM does not allow calculations with high accuracy.

In [14–16], for modeling the SSC of objects, the method of finite differences in the time domain (FDTD) was proposed, which is based on a discrete analogue of exact equations. The advantages of this method are the calculation of the EMF at successive points in time, simulating a real physical process and the high accuracy of the calculations. However, this also determines its disadvantages – the need to introduce limiting conditions that eliminate reflection from the boundaries of the calculation area that do not exist in reality, large volumes and costs of calculations.

To calculate the SSC of resonant objects, the surface of which can be considered ideally conducting (IC), in free space, a calculation method based on the solution of the integral magnetic field equation (IMFE) is used [17–19].

While for a dielectric object of resonant dimensions located in a homogeneous space, the method of calculating the SSC is based on the solution of the Müller-type IE system, which is given in [20–22]. The advantage of using IE is the ability to determine the scattered EMF at an arbitrary point in space with high accuracy through known fields inside the object or on its surface. In the above works, the dependences of the secondary characteristics of IC or dielectric objects on their angles were obtained. However, these papers do not consider the situation of bistatic probing of combined objects of resonant sizes with the electrophysical properties of biological tissues, which is typical for covert detection in the ISF protection zone.

Thus, the analysis of the sources showed the need for theoretical studies related to obtaining bistatic secondary characteristics of radar scattering of combined objects of resonant sizes with electrophysical properties of biological tissues and analyzing their dependencies.

The aim of research is to obtain secondary characteristics of the bistatic scattering of a combined object (an intruder in the PAP) in a covert radar surveillance system and to analyze them.

To achieve the aim, it is necessary to solve the following objectives:

1. To develop a methodology for estimating the effective scattering surface of combined objects of complex shape in the field of illumination of television and cellular networks.

2. To obtain the results of mathematical modeling and analyze the effective scattering surface of combined objects of complex shape.

3. To verify the calculation results.

2. Materials and methods

2. 1. Development of a methodology for estimating the effective scattering surface of combined objects in the backlight field of television and cellular networks

A specific method for modeling the scattering characteristics of combined objects is determined by the electrodynamic characteristics of the materials of the elements of objects, their electrical dimensions and shape. The combined object is typically a complex object having both metallic and dielectric elements. EMF scattered by a combined object in the meter and decimeter wavelength ranges can be calculated as a coherent sum of fields scattered by its elements. The sum of the scattered EMFs of individual metal and dielectric elements of the combined object, taking into account their phase, makes it possible to take into account their electromagnetic interaction.

Let's establish the condition of equality to zero of the primary field at the receiving point $\vec{Q}_{np}$. Then, using integral representations for the strength of the field components scattered by metal $\vec{H}^{np}_{met}\left(\vec{Q}_{np}\right)$ and dielectric objects $\vec{H}^{np}_{met}\left(\vec{Q}_{np}\right)$, the expression for the strength of the magnetic field scattered by the combined object can be written in the following form:

$$\vec{p}^{np}\cdot\vec{H}^{np}\left(\vec{Q}_{np}\right)=\vec{p}^{np}\cdot\left(\vec{H}^{np}_{met}\left(\vec{Q}_{np}\right)+\vec{H}^{np}_{diel}\left(\vec{Q}_{np}\right)\right). \quad (1)$$

The intensity of the magnetic field $\vec{H}^{np}_{met}\left(\vec{Q}_{np}\right)$ scattered by the metal elements of the desired object V_2 in the homogeneous space V_1 can be determined using the integral representation [23]:

$$\vec{p}^{np}\cdot\vec{H}^{np}_{met}\left(\vec{Q}_{np}\right)=-\frac{1}{i\omega}\int\limits_{S_{met}}\vec{\mathrm{E}}^{m}_{1}\left(\vec{Q}\middle|\vec{Q}_{np},\vec{p}^{np}\right)\cdot\vec{J}^{e}_{met}\left(\vec{Q}\right)ds_Q, \quad (2)$$

where $\vec{p}^{np}$ – unit vector indicating the direction in which the scattered field vector is projected $\vec{H}^{np}$; S_{met} – set of particles of metal surfaces; $\vec{J}^{e}_{met}$ – electric current density on the particles of metal surfaces; $\vec{Q}_{np}\in V_1$ ($\vec{Q}_{np}\notin V_2\bigcup S$) – point at which the scattered field is calculated.

To calculate the electric current density $\vec{J}^{e}_{met}\left(\vec{Q}\right)$ on the surface of the IC elements, IMFE is used [23]:

$$\left(\vec{\nu}^0\times\vec{\tau}^0_q\right)\cdot\vec{J}^{e}_{met}\left(\vec{Q}_0\right)\left(1+\Omega_{s_0}\left(\vec{Q}_0\right)\right)+\frac{2}{i\omega}\int\limits_{S_{met}\setminus s_0}\vec{\mathrm{E}}^{m}_{1}\left(\vec{Q}\middle|\vec{Q}_0,\vec{\tau}^0_q\right)\cdot\vec{J}^{e}_{met}\left(\vec{Q}\right)ds_Q=2\vec{\tau}^0_q\cdot\vec{\mathrm{H}}^0_1\left(\vec{Q}_0\right), \quad (3)$$

where $\vec{Q}_0$, $\vec{Q}\in S_{met}$ – points of observation and integration, respectively; $\vec{\nu}^0$ – unit vector of the internal normal to the surface S_{met} at a point $\vec{Q}_0$; $\vec{\tau}^0_q$ ($q=1, 2$) – involved in S_{met} unit vectors at the point $\vec{Q}_0$ forming the right triple with the normal vector $\vec{\nu}^0$; $\vec{\mathrm{H}}^0_1\left(\vec{Q}_0\right)$ – intensity of the primary magnetic field; $\vec{\mathrm{E}}^{m}_{1}\left(\vec{Q}\middle|\vec{Q}_0,\vec{\tau}^0_q\right)$ – electric field strength (at a point $\vec{Q}$) of a point magnetic dipole (with a vector-moment $\vec{\tau}^0_q$, located at a point $\vec{Q}_0$ of free space V_1); $\Omega_{s_0}\left(\vec{Q}_0\right)$ is the following expression:

$$\Omega_{s_0}\left(\vec{Q}_0\right)=2(i\omega)^{-1}\int\limits_{s_0}\vec{\mathrm{E}}^{m}_{1}\left(\vec{Q}\middle|\vec{Q}_0,\vec{\tau}^0_q\right)ds_Q\approx\frac{c_1+c_2}{2ik_1}\left[(ik_1\rho_0-2)\exp(ik_1\rho_0)+2\right], \quad (4)$$

where $k_\alpha=\omega\sqrt{\varepsilon_0\varepsilon_\alpha\mu_0}=2\pi/\lambda_\alpha$ – wavenumber in the medium V_α with relative permittivity ε_α; λ_α – wavelength in V_α; ε_0, μ_0 – absolute dielectric and magnetic permeability of free space, respectively; s_0 – element of the surface S_{met}, located inside a sphere of small radius $\rho_0\ll\lambda_1$ centered at the point; $\vec{Q}_0$; c_q ($q=1, 2$) is the following expression:

$$c_q = \frac{\partial^2 F\left(\vec{Q}(u_1, u_2)\right)}{\partial u_q^2}\left(\vec{\tau}_q^0\right)^2 \Bigg/ \left[2\left|\nabla F\left(\vec{Q}(u_1, u_2)\right)\right|_{\vec{Q}=\vec{Q}_0}\right], \quad (5)$$

where (u_1,u_2) – local rectangular coordinate system centered at the point $\vec{Q}_0$, which axes are directed along $\vec{\tau}_1^0$, $\vec{\tau}_2^0$, respectively; $F\left(\vec{Q}(u_1, u_2)\right) = 0$ – equation of the surface S_{met} in the small outskirts of the point $\vec{Q}_0$.

The intensity of the magnetic field $\vec{H}_{diel}^{np}\left(\vec{Q}_{np}\right)$ scattered by the dielectric elements of the object V_2 in the homogeneous space V_1 is determined [24]:

$$\vec{p}^{np} \cdot \vec{H}_{diel}^{np}\left(\vec{Q}_{np}\right) = -\frac{1}{i\omega}\int\limits_{S_{diel}} \left[\Delta\vec{\mathrm{H}}_{21}^{m}\left(\vec{p}^{np}\right)\cdot\vec{J}_{diel}^{m}\left(\vec{Q}\right) + \Delta\vec{\mathrm{E}}_{21}^{m}\left(\vec{p}^{np}\right)\cdot\vec{J}_{diel}^{e}\left(\vec{Q}\right)\right] ds_Q, \quad (6)$$

where S_{diel} – set of particles of dielectric surfaces; $\vec{J}_{diel}^{e}$, $\vec{J}_{diel}^{m}$ – density of electric and magnetic currents on particles of dielectric surfaces.

The densities of the equivalent magnetic $\vec{J}_{diel}^{m}$ and electric $\vec{J}_{diel}^{e}$ currents on the surface S_{diel} of the object V_2 can be found using the system of Muller-type integral equations (SIEM) [24]:

$$\begin{cases} \left(\vec{\tau}_q^0 \times \vec{\nu}^0\right)\cdot\vec{J}_{diel}^{m}\left(\vec{Q}_0\right)\left(\varepsilon_1+\varepsilon_2\right) + 2(i\omega)^{-1} \times \\ \times \int\limits_{S_{diel}} \left[\Delta\vec{\mathrm{H}}_{21}^{e}\left(\vec{\tau}_q^0\right)\cdot\vec{J}_{diel}^{m}\left(\vec{Q}\right)\varepsilon_2 + \varepsilon_0^{-1}\Delta\vec{\mathrm{D}}_{21}^{e}\left(\vec{\tau}_q^0\right)\cdot\vec{J}_{diel}^{e}\left(\vec{Q}\right)\right] ds_Q = -2\varepsilon_1\vec{\tau}_q^0\cdot\vec{\mathrm{E}}_1^0\left(\vec{Q}_0\right), \\ -\left(\vec{\tau}_q^0 \times \vec{\nu}^0\right)\cdot\vec{J}_{diel}^{e}\left(\vec{Q}_0\right) + (i\omega)^{-1} \times \\ \times \int\limits_{S_{diel}} \left[\Delta\vec{\mathrm{H}}_{21}^{m}\left(\vec{\tau}_q^0\right)\cdot\vec{J}_{diel}^{m}\left(\vec{Q}\right) + \Delta\vec{\mathrm{E}}_{21}^{m}\left(\vec{\tau}_q^0\right)\cdot\vec{J}_{diel}^{e}\left(\vec{Q}\right)\right] ds_Q = \vec{\tau}_q^0\cdot\vec{H}_1^0\left(\vec{Q}_0\right). \end{cases} \quad (7)$$

In the case of a dielectric scatterer, when $\vec{\nu}^0$ represents the components of the expressions of system (7) external to the Sdiel normal, are calculated as:

$$\Delta\vec{\mathrm{H}}_{21}^{e}\left(\vec{Q}\middle|\vec{Q}_0,\vec{\tau}_q^0\right) \equiv \Delta\vec{\mathrm{H}}_{21}^{e}\left(\vec{\tau}_q^0\right) = \vec{\mathrm{H}}_2^{e}\left(\vec{Q}\middle|\vec{Q}_0,\vec{\tau}_q^0\right) - \frac{\varepsilon_1}{\varepsilon_2}\vec{\mathrm{H}}_1^{e}\left(\vec{Q}\middle|\vec{Q}_0,\vec{\tau}_q^0\right),$$

$$\Delta\vec{\mathrm{D}}_{21}^{e}\left(\vec{Q}\middle|\vec{Q}_0,\vec{\tau}_q^0\right) \equiv \Delta\vec{\mathrm{D}}_{21}^{e}\left(\vec{\tau}_q^0\right) = \vec{\mathrm{D}}_2^{e}\left(\vec{Q}\middle|\vec{Q}_0,\vec{\tau}_q^0\right) - \vec{\mathrm{D}}_1^{e}\left(\vec{Q}\middle|\vec{Q}_0,\vec{\tau}_q^0\right),$$

$$\Delta\vec{\mathrm{H}}_{21}^{m}\left(\vec{Q}\middle|\vec{Q}_0,\vec{\tau}_q^0\right) \equiv \Delta\vec{\mathrm{H}}_{21}^{m}\left(\vec{\tau}_q^0\right) = \vec{\mathrm{H}}_2^{m}\left(\vec{Q}\middle|\vec{Q}_0,\vec{\tau}_q^0\right) - \vec{\mathrm{H}}_1^{m}\left(\vec{Q}\middle|\vec{Q}_0,\vec{\tau}_q^0\right),$$

$$\Delta\vec{\mathrm{E}}_{21}^{m}\left(\vec{Q}\middle|\vec{Q}_0,\vec{\tau}_q^0\right) \equiv \Delta\vec{\mathrm{E}}_{21}^{m}\left(\vec{\tau}_q^0\right) = \vec{\mathrm{E}}_2^{m}\left(\vec{Q}\middle|\vec{Q}_0,\vec{\tau}_q^0\right) - \vec{\mathrm{E}}_1^{m}\left(\vec{Q}\middle|\vec{Q}_0,\vec{\tau}_q^0\right),$$

where $\left(\vec{\mathrm{E}}_{1(2)}^{e(m)}, \vec{\mathrm{H}}_{1(2)}^{e(m)}\right)$ – components of the EMF of electric (magnetic) point dipoles, provided that the regions V_1 and V_2 filled with a homogeneous material with a permittivity проникністю $\varepsilon_{1(2)}$; $\vec{\mathrm{D}}_\alpha^e = \varepsilon_0\varepsilon_\alpha\vec{\mathrm{E}}_\alpha^e$ – electric induction vector of the electric dipole field.

IMFE (3) and SIEM (7) are discretized and reduced to the corresponding systems of linear algebraic equations. The surface of both the IC and the dielectric diffuser is approximated by segments of ellipsoids. For a more detailed account of the electromagnetic interaction of metallic and dielectric elements of a combined object, iterative methods can be used [25].

2. 2. Problem statement of modeling the bistatic effective scattering surface of combined objects

The geometric formulation of the modeling problem is shown in **Fig. 1**. In the free half-space V_1 at the interface $z = 0$ there is a combined object V_2 with the surface S, which is a combination of IC and dielectric elements. Regions V_1, V_2 have corresponding relative permeabilities $\varepsilon_1 = 1$, $\varepsilon_2 = \varepsilon_2' + i\varepsilon_2''$. With a dielectric element of an object, the complex permeability ε_2 is a function of frequency. In the case of a metal element $\varepsilon_2'' \to \infty$. Relative magnetic permeability μ is equal to 1 in all areas. The EMF inside the object is zero. Object V_2 is irradiated by transmitter antenna T2 (point A_1), generating EMF $\left(\vec{\mathrm{E}}^0, \vec{\mathrm{H}}^0\right)$. The reflected signal is received by the passive radar antenna (point A_2).

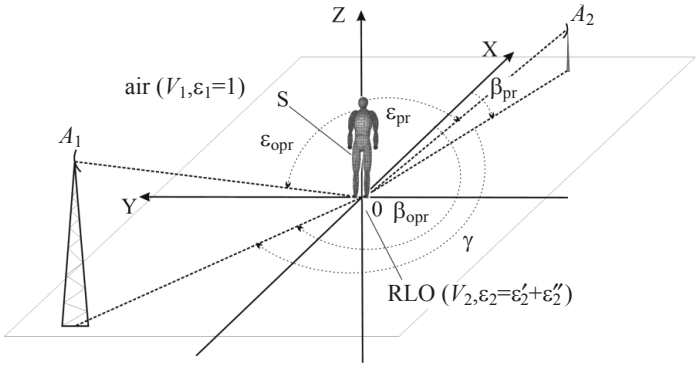

Fig. 1. Conditions for irradiation and reception of the signal reflected by the object

The mutual arrangement of the receiver and transmitter is characterized in the azimuthal plane by a bistatic angle γ. The impact of the height of the receiving and transmitting antennas is taken into account by the angles ε_{pr} and ε_{opr} in the elevation plane, respectively. Some frequencies of digital packets MX of terrestrial television T2 for the CIS countries and Europe (f_0 = 586 MHz, 706 MHz) and the frequency of mobile communications GSM-900 (f_0 = 900 MHz) were used as the ambient illumination frequency.

In the study, as an example, the height of the receiving antenna is 3 m, the height of the external illumination repeater is 72 m. The distance between the A_2 receiver and the A_1 transmitter is 25 km. The observation object is located at a distance of 5 km from the A_2 receiver.

The most important component of mathematical methods for calculating the characteristics of radar scattering of objects are three-dimensional digital models of their surfaces. In the work, methods for creating models of surfaces of resonant objects of complex shape, adapted to the proposed methods for solving IE [26], were used. These methods of creating a surface model make it possible to obtain sTable results of calculations of the scattering characteristics of resonant objects of complex shape with a smaller number of elementary sections of the surface scatterer than other methods.

Table 1 shows the main biometric characteristics of the intruder and the characteristics of personal armor protection.

Table 1

Characteristics of the perpetrator and the PAP

Characteristic	Value, m
Intruder face	
Growth	1.8
Width	0.65
Thickness	0.21
Means of personal armor protection	
Army helmet diameter	0.26
Depth	0.17
Armor elements of body armor	0.3×0.25

Fig. 2 shows the appearance (*a*), the surface model of the intruder's face (*b*) and the intruder's face in the PAP (*c*).

The intruder is a dielectric object with permeability parameters of biological tissues, the surface of which is approximated by sections of 22 dielectric ellipsoids. The intruder in the PAP is a combined object, consisting of sections of 20 dielectric ellipsoids and 2 IC (helmet and body armor).

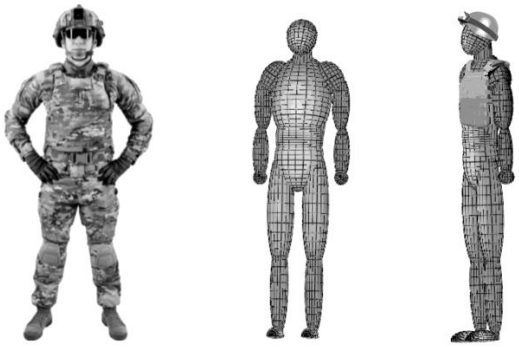

a *b* *c*

Fig. 2. Model of the personality-intruder: *a* – appearance; *b* – surface model of the intruder; *c* – model of the surface of the intruder's face in personal armor protection

3. Results and discussion

During the simulation, the results of calculating the scattering diagrams of the person-intruder and the person-intruder in the PAP were obtained under various conditions of irradiation and reception and at different frequencies of external illumination. The bistatic scattering diagram of an object means the dependence of its RCS on the bistatic separation angle in the azimuthal plane.

In addition, when modeling the bistatic scattering diagram of the objects considered in the study, the following restrictions and application conditions are established:

– areas of ellipsoids of the surface of radar objects are considered as a homogeneous layer (metal or dielectric);

– the values of the dielectric constant of a biological object as a whole are calculated as a proportional sum of the permeabilities of the types of biological tissues emitted in the object in the range of meter and decimeter waves (f_0 from 100 MHz to 1 GHz);

– RCS calculation of the object is carried out in the forward hemisphere, which corresponds to the features of the ISF protection;

– RCS calculation is performed without taking into account the impact of the underlying surface (that is, in free space). As the research results show, the influence of the underlying surface leads to RCS fluctuations relative to the case of free space [27];

– when modeling, it was assumed that the signal reflected from the earth's surface in the radar receiver was compensated using known algorithms for suppressing reflections from local objects [11].

The results are considered as some average values, allowing to estimate the level of the scattered signal. Such data correspond to the case of a rather narrow radiation pattern of the receiving antenna of a passive radar in the elevation plane.

The calculations were made at the frequency of the digital television package T2 $f_0 = 586$ MHz ($\lambda_0 \approx 0.512$ m). The sounding azimuths β_{opr} were chosen to be 1800 and 2100, respectively. **Fig. 3** shows bistatic scatterplots of the intruder's face (blue lines) and **Fig. 4** intruder in the PAP (red lines).

Tables 2, 3 show the average values of RCS, and in **Tables 4, 5** show the medians EES of the intruder (the numerator of the fraction) and the intruder in the PAP (the denominator of the fraction), in the sectors of bistatic angles at the corresponding irradiation azimuths.

As evidenced by the results shown in **Fig. 3, 4** and in **Tables 2–5**, the bistatic RCS of objects at a given frequency and considered illumination azimuths depend on the EMF polarization. The energy gain in sounding these objects is obtained by using VP waves, regardless of the direction of reception and sounding. This effect is due to the fact that the electrical dimensions of the intruder in the vertical plane are much larger than in the horizontal. In addition, at the considered wavelengths, the scattering diagram of objects is smooth. The effect of the so-called «enlightening» location is manifested in the range of bistatic angles from 165° to 195°, where the RCS increases significantly and can reach median values of 18.94/21.07 m^2 (**Table 4**). Moreover, an increase in the values of the bistatic RCS is observed at all angles of illumination by the T2 transmitter.

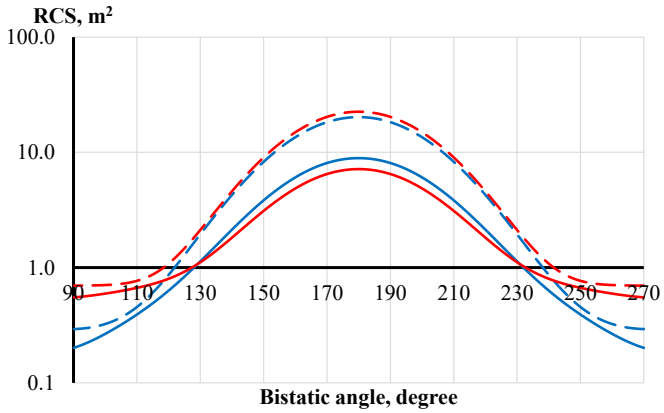

Fig. 3. Bistatic radar cross-section of objects at $f_0 = 586$ MHz, $\beta_{opr} = 180°$

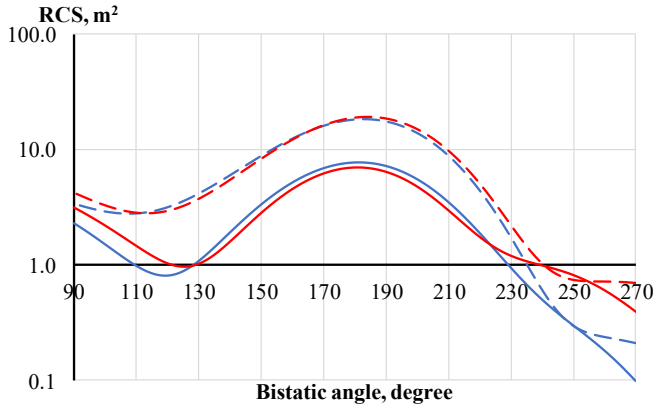

Fig. 4. Bistatic radar cross-section of objects at $f_0 = 586$ MHz, $\beta_{opr} = 210°$

Table 2

Average bistatic RCS of objects at $f_0 = 586$ MHz, $\beta_{opr} = 180°$

Polarization	RCS value, m²				
	Bistatic angle				
	90…134 deg.	135…164 deg.	165...195 deg.	196...225 deg.	226…270 deg.
horizontal	0.56/0.76	3.93/3.20	8.26/6.63	3.93/3.20	0.56/0.76
vertical	0.82/1.11	8.51/9.32	18.69/20.78	8.51/9.32	0.82/1.11

Table 3

Average bistatic RCS of objects at $f_0 = 586$ MHz, $\beta_{opr} = 210°$

Polarization	RCS value, m²				
	Bistatic angle				
	90…134 deg.	135…164 deg.	165...195 deg.	196...225 deg.	226…270 deg.
horizontal	1.22/1.62	3.40/2.92	7.16/6.42	3.54/3.09	0.43/0.84
vertical	3.24/3.29	8.90/8.48	17.01/17.65	8.80/9.69	0.65/1.11

Table 4

Median bistatic RCS of objects at $f_0 = 586$ MHz, $\beta_{opr} = 180°$

Polarization	RCS value, m²				
	Bistatic angle				
	90…134 deg.	135…164 deg.	165...195 deg.	196...225 deg.	226…270 deg.
horizontal	0.43/0.69	3.73/3.03	8.37/6.72	3.73/3.03	0.43/0.69
vertical	0.51/0.80	8.03/8.77	18.94/21.07	8.03/8.77	0.51/0.80

Table 5

Median bistatic RCS of objects at $f_0 = 586$ MHz, $\beta_{opr} = 210°$

Polarization	RCS value, m²				
	Bistatic angle				
	90…134 deg.	135…164 deg.	165...195 deg.	196...225 deg.	226…270 deg.
horizontal	1.08/1.34	3.24/2.73	7.27/6.53	3.39/2.87	0.33/0.85
vertical	3.05/3.15	8.60/8.10	17.34/18.04	8.54/9.46	0.32/0.76

When illuminated, $\beta_{opr} = 180°$ relative to $\gamma = 180°$, axial symmetry of the obtained EPR diagrams is observed (**Fig. 3**). When the direction of illumination β_{opr} is changed, the symmetry of the dependences disappears and it is necessary to consider certain sectors of azimuths. So, at $\beta_{opr} = 210°$ (**Fig. 4**), there is an increase in the RCS value at bistatic angles of 90–134° by 2–3 times with an average RCS value of 1.22/1.62 (HP) and 3.24/3, 29 m² (VP). This effect is explained by the fact that in the range of angles 90°–134° the «illuminated» surface area of the intruder increases.

When calculating the RCS of the intruder's personality in the PAP, it is possible to observe the IC influence of the object's parts on the RCS value. This is especially manifested also in VP, there is an increase in EPR in almost all ranges by 10–15 %. And in the ranges of 90–134° and 226–270°, the increase in RCS can reach up to 35 %. However, with VP in the range of 130–230°, a decrease in RCS by up to 30 % is observed. Such an influence of the IC parts of the model is explained by the absence of EMF absorption in the IC parts of the model, the appearance of resonance effects, and a change in the phase of the reflected wave. **Fig. 5** shows the bistatic scatterplots of the intruder personality and in **Fig. 6** intruders in the PAP with various sources of illumination at the frequencies of the T2 digital television package – 706 MHz ($\lambda_0 \approx 0.425$ m) and GSM mobile communications –900 MHz ($\lambda_0 \approx 0.333$ m). The calculations were carried out at the irradiation azimuth $\beta_{opr} = 180°$.

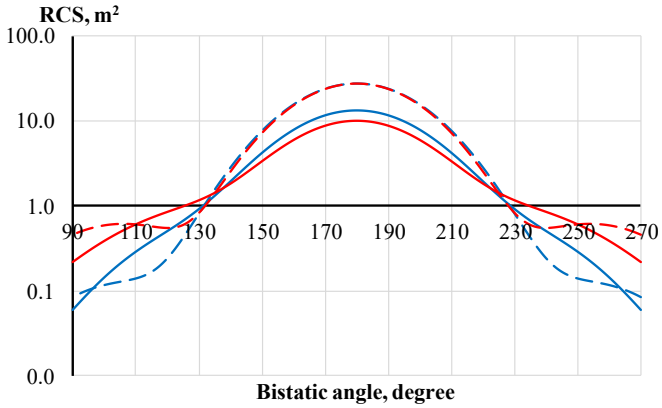

Fig. 5. Bistatic radar cross-section of objects at $f_0 = 706$ MHz, $\beta_{opr} = 180°$

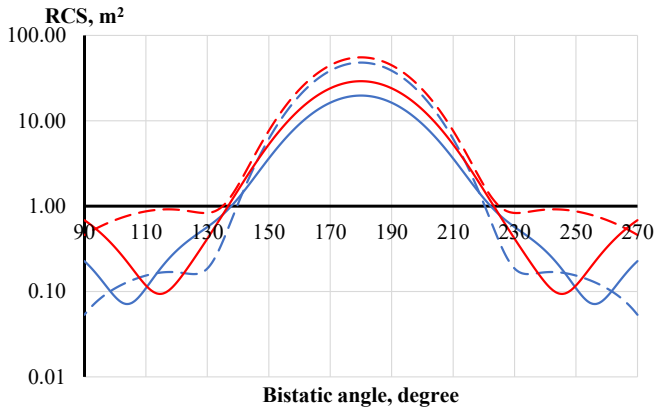

Fig. 6. Bistatic radar cross-section of objects at $f_0 = 900$ MHz, $\beta_{opr} = 180°$

Tables 6, 7 show the average values of RCS, and **Tables 8, 9** – the median value of the RCS of the objects under consideration in the sectors of bistatic angles at the corresponding frequencies.

Table 6

Average bistatic RCS of objects at $f_0 = 706$ MHz, $\beta_{opr} = 180°$

Polarization	RCS value, m²				
	Bistatic angle				
	90…134 deg.	135…164 deg.	165...195 deg.	196...225 deg.	226…270 deg.
horizontal	0.41/0.69	4.57/3.65	12.0/9.06	4.57/3.65	0.41/0.69
vertical	0.30/0.63	8.49/8.13	24.71/24.61	8.49/8.13	0.30/0.63

Table 7

Average bistatic RCS of objects at $f_0 = 900$ MHz, $\beta_{opr} = 180°$

Polarization	RCS value, m²				
	Bistatic angle				
	90…134 deg.	135…164 deg.	165...195 deg.	196...225 deg.	226…270 deg.
horizontal	0.26/0.30	4.57/6.63	17.11/25.23	4.57/6.63	0.26/0.30
vertical	0.15/0.79	8.79/10.68	40.89/47.26	8.79/10.68	0.15/0.79

Table 8

Median bistatic RCS of objects at $f_0 = 706$ MHz, $\beta_{opr} = 180°$

Polarization	RCS value, m²				
	Bistatic angle				
	90…134 deg.	135…164 deg.	165...195 deg.	196...225 deg.	226…270 deg.
horizontal	0.32/0.65	4.06/3.25	12.20/9.21	4.06/3.25	0.32/0.65
vertical	0.15/0.59	7.34/6.89	25.15/25.06	7.34/6.89	0.15/0.59

Table 9

Median bistatic RCS of objects at $f_0 = 900$ MHz, $\beta_{opr} = 180°$

Polarization	RCS value, m²				
	Bistatic angle				
	90…134 deg.	135…164 deg.	165...195 deg.	196...225 deg.	226…270 deg.
horizontal	0.19/0.24	3.44/5.00	17.48/25.78	3.44/5.00	0.19/0.24
vertical	0.16/0.84	5.72/7.16	41.87/48.38	5.72/7.16	0.16/0.84

Comparison of the obtained simulation data indicates an increase in the intensity of the secondary radiation of objects with an increase in the illumination frequency. Especially this increase is observed at a frequency of $f_0 = 900$ MHz, where the average EPR in the range of bistatic angles of 150–190° is 3–4 times higher than similar indicators at other frequencies. With an increase in the illumination frequency, a decrease in the width of the central peak, in which the effect of «illumination» location is manifested, is observed, down to 600 and the appearance of insignificant new RCS peaks in the ranges of 90–130 and 240–270 (**Fig. 6**).

With an increase in the illumination frequency, the IC influence of parts of the intruder's model is similar to that analyzed earlier (**Fig. 3**). However, in the ranges of 90–134°, 226–270° at a frequency of 706 MHz, the ratio of the average values of the RCS of the intruder in the PAP and the intruder is 1.48 times (HP) and 2.1 (VP), at 900 MHz-5.26 (VP). In addition, with an increase in frequency, the maximum value of the RCS of the intruder and the intruder in the PAP also increases significantly, which is given in **Table 10**.

Table 10

The maximum value of the bistatic RCS of the intruder at different backlight frequencies

Polarization	Maximum RCS value, m^2				
	Backlight frequency				
	474 MHz	**506 MHz**	**586 MHz**	**706 MHz**	**900 MHz**
horizontal	6.36/5.41	7.04/5.87	8.91/7.15	13.29/10.04	19.78/29.15
vertical	15.00/17.17	16.43/18.37	20.21/22.51	27.54/27.52	48.17/55.47

At a frequency of $f_0 = 900$ MHz, the RCS on the HP and VP in the range of bistatic angles of 170–190° differ significantly. On HP, in contrast to VP, a surge of values is approximately 2–2.5 times less. They are about 19.78 m^2 for a human intruder and 29.15 m^2 for a human intruder in the PAP. When on the VP – 48.17 m^2 and 55.47 m^2, respectively.

Based on the above, it is advisable to build a covert surveillance system using bistatic angles in the range of 165–195° at the VP of the probing signal. As a receiving antenna, it is necessary to use an antenna with a beam width in azimuth from 30° to 60°.

To confirm the reliability of these calculations, a check for convergence and verification of the results was carried out on the example of an object of a simple shape.

When calculating the RCS, the number of nodes N of the discrete grid on the surface of the intruder, in which the current density was calculated, was chosen in such a way that there was an internal convergence of the algorithm, characterized by a given value of δ_a. Moreover, starting from some values $N = N_a$, the following condition is fulfilled:

$$\delta = \frac{\left|\sigma_{N_c} - \sigma_{N_a}\right|}{\sigma_{N_c}} \cdot 100\ \% \le \delta_a, \tag{8}$$

where σ_{N_a}, σ_{N_c} – RCS values calculated for the number of nodes N_a and N_c, respectively, and $N_c > N_a$. In calculations, the number of nodes N_a was chosen corresponding to $\delta_a < 3$ %.

When sounding an object with an azimuth of 180° at a frequency of 586 MHz in **Table 11** it is shown that the value in the range of bistatic angles 176…184° for the number of nodes of the discrete grid of the object surface: 2138 and 2542.

Table 11

The value of δ in the range of bistatic angles for the intruder face

Bistatic angle, degree	176	177	178	179	180	181	182	183	184
HP, %	0.94	0.95	0.96	0.97	0.97	0.97	0.96	0.95	0.94
VP, %	1.65	1.65	1.66	1.66	1.66	1.66	1.66	1.65	1.65

In addition, the verification of the results of this technique was carried out on the example of objects of a simple shape – IC ball with a radius of $r = 2$ meters. In [28], the dependence of the mean RCS on the bistatic angle was analytically shown. When γ reaches 180°, its sharp increase takes place and is calculated by expression (9):

$$\bar{\sigma}(\gamma = 180°) = 4\pi^3 r^4 \lambda^{-2}. \tag{9}$$

The plots of the dependences of the RCS values obtained by the IE method for the HP (solid line) and the VP (dashed line) for frequencies $f_0 = 586$ MHz and 900 MHz are shown in **Fig. 7**.

The obtained calculated values of the bistatic RCS (**Fig. 7**) are in full agreement with the theory. Comparisons of the results of analytical calculations and those obtained by the proposed IE method at the characteristic point $\gamma = 180°$ are given in **Table 12**.

The relative error in calculating the bistatic EPR of the IC ball at $\gamma = 180°$ reaches 1–3 %, which indicates the reliability of the proposed method.

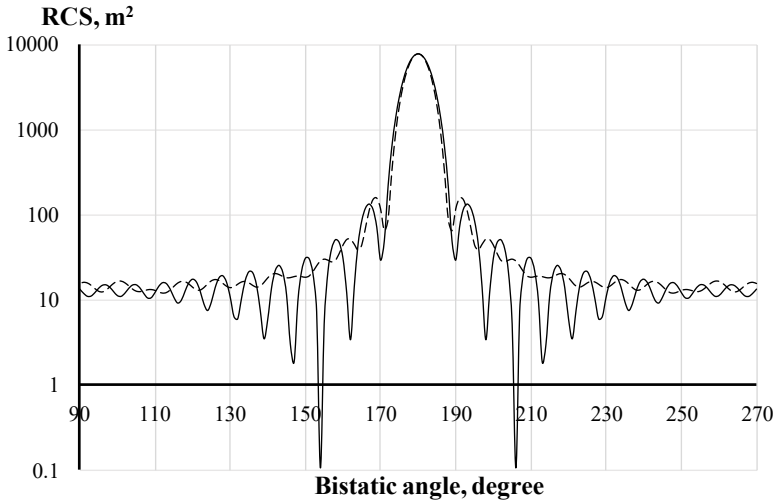

a

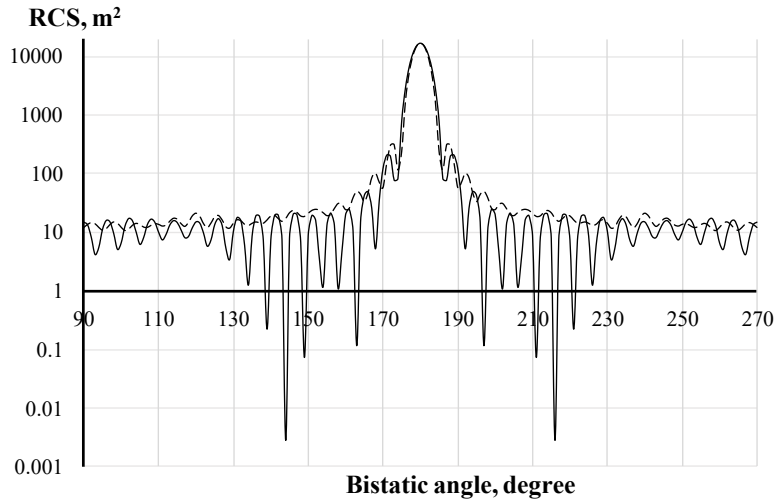

b

Fig. 7. Bistatic radar cross-section for a discrete grid with 2542 surface nodes of a perfectly conducting ball with a radius of 2 m for two polarizations: *a* – f_0 = 586 MHz; *b* – f_0 = 900 MHz

Table 12

Comparison of the obtained values of bistatic RCS

Parameters	f_0 = 586 MHz		f_0 = 900 MHz	
	HP	VP	HP	VP
RCS analytical calculation, m²	7571.5	7571.5	17859.61	17859.6
RCS IC method, m²	7816.11	7816.05	17645.45	17644.9
relative error, %	3.22	3.22	1.20	1.20

The further direction of development of the research should be focused on taking into account the electromagnetic interaction between the IC and dielectric elements directly in IE for the current densities on the surfaces of these dissimilar elements. This will make it possible to obtain a more accurate value of the characteristics of the secondary radiation of resonant combined objects.

4. Conclusions

1. A technique for estimating the effective scattering surface of combined objects of complex shape in the backlight field of television and cellular networks is given, taking into account

the electrodynamic characteristics of the materials of the elements of objects, their electrical dimensions and shape. The electromagnetic field scattered by the combined object in the meter and decimeter wavelength ranges is calculated as a coherent sum of the fields scattered by its elements. The sum of the scattered electromagnetic fields of individual metal and dielectric elements of the combined object based on the phase makes it possible to take into account their electromagnetic interaction in the first approximation.

The use of this technique makes it possible to obtain a priori information about the secondary characteristics of the radiation of combined objects of various designs under various conditions of radar observation without significant financial costs and material resources. This information is of significant practical importance at the stage of optimizing signal processing algorithms and designing new means of covert detection.

2. Scattering diagrams of two complex-shaped objects were obtained and analyzed under different irradiation and reception conditions and at different external illumination frequencies. As objects of modeling, an intruder face (a dielectric object with biological tissue permeability parameters) and an intruder in the PAP (combined object) were chosen. This allowed the influence of the IC elements (helmet and body armor) on the scatter diagram of the object.

Energy gain is obtained when using VP waves, regardless of the direction of reception and sounding. This is due to the fact that the electrical dimensions of the studied objects in the vertical plane are much larger than in the horizontal. The effect of the so-called «enlightening» location is manifested in the range of bistatic angles from 165° to 195°, where the RCS increases significantly and can reach median values of 18.94/21.07 m^2 at $f_0 = 586$ MHz. With an increase in the illumination frequency, an increase in the intensity of the secondary radiation of objects is also observed. Especially this increase is observed at a frequency of = 900 MHz, where the average RCS in the range of bistatic angles of 150–190° is 3–4 times higher than similar indicators at other frequencies.

The value of the RCS of the combined object during VP increases by 10–15 % in almost all ranges. And in the ranges of 90–134° and 226–270°, the increase in RCS can reach up to 35 %. However, with HP in the range of 130–230°, a decrease in RCS by up to 30 % is observed. Such an influence of the IC parts of the model is explained by the absence of EMF absorption in the IC parts of the model, the appearance of resonance effects, and a change in the phase of the reflected wave. With an increase in the backlight frequency, the influence of the IC of parts of the intruder personality model on the RCS value also increases, especially in the ranges of 90–134° and 226–270°. So, at a frequency of 706 MHz, the ratio of the average values of the RCS of the intruder and the intruder in the PAP is 1.48 times (HP) 2.1 (VP), at a frequency of 900 MHz – 5.26 times (VP).

3. To confirm the reliability of these calculations, a check for convergence and verification of the results was carried out using the example of an IC ball. At the same time, it was found that 2542 nodes of a discrete grid of the surface of these objects are sufficient for calculating the RCS by the IE method with a convergence of no more than 3 %. In addition, the calculated values of the bistatic RCS by the IE method are in complete agreement with the theory. The relative error in calculating the bistatic RCS of the IC ball by the analytical method and the IE method at the characteristic point $\gamma = 180°$ reaches 1–3 %, which indicates the reliability of the proposed method.

References

[1] Horielyshev, S., Volkov, P. (2021). Ways to improve the security system of important state objects. The Scientific Journal of the National Academy of National Guard «Honor and Law», 1 (76), 40–45. doi: https://doi.org/10.33405/2078-7480/2021/1/76/229506

[2] Syrotenka A. M. (2020). Voienni aspekty protydiyi «hibrydniy» ahresiyi: dosvid Ukrainy. Kyiv, 176. Available at: https://nuou.org.ua/assets/monography/mono_gibr_viin.pdf

[3] Horielyshev, S., Volkov, P., Oleschenko, O. (2021). Characteristics of radar scattering of the violating person in the system of hidden radar observation. The Scientific Journal of the National Academy of National Guard «Honor and Law», 4 (79), 20–32. doi: https://doi.org/10.33405/2078-7480/2021/4/79/251495

[4] Horielyshev, S., Boikov, I., Volkov, P., Poberezhnyi, A., Kondratenko, A. (2021). Comparison of the parameters of signals with external illumination for supervision of the area for the protection of important state objects. EUREKA: Physics and Engineering, 1, 14–23. doi: https://doi.org/10.21303/2461-4262.2021.001607

[5] Barkhatov, A. V., Verem'ev, V. I., Vorob'ev, E. N. (2016). Passivnaya kogerentnaya radiolokatsiya. Sankt-Peterburg, 163. Available at: https://etu.ru/assets/files/nauka/nii/Prognoz/Publikatcii/2017-passiv-kogerent-radiolok-2016.pdf

[6] Mayzel's, E. N., Torgovanov, V. A. (1972). Izmerenie kharakteristik rasseyaniya radiolokatsionnykh tseley. Moscow, 232. Available at: https://goo.su/Xmn

[7] Howland Company. Available at: https://thehowlandcompany.com/

[8] Knott, E. F., Shaeffer, J. F., Tuley, M. T. (2004). Radar Cross Section. Institution of Engineering and Technology. doi: https://doi.org/10.1049/sbra026e

[9] L'vova, L. A. (2003). Radiolokatsionnaya zametnost' letatel'nykh apparatov. Snezhinsk: RFYATS. Available at: https://ru.ua1lib.org/book/3015992/c996c6

[10] Ufimtsev, P. Y. (20009). Theory of Edge Diffraction in Electromagnetics: Origination and validation of the physical theory of diffraction. Institution of Engineering and Technology. doi: https://doi.org/10.1049/sbew054e

[11] Skolnik, M. I. (2008). Radar Handbook. McGraw-Hill. Available at: https://ftp.idu.ac.id/wp-content/uploads/ebook/tdg/ADNVANCED%20MILITARY%20PLATFORM%20DESIGN/Radar%20Handbook.pdf

[12] Gibson, W. C. (2008). The Method of Moments in Electromagnetics. Boca Raton. Available at: http://www.lmn.pub.ro/~daniel/ElectromagneticModelingDoctoral/Books/BEM%20MoM/Gibson%20MoM%20in%20Electromagnetics.pdf

[13] Sukharevsky, O. I. (Ed.) (2018). Electromagnetic Wave Scattering by Aerial and Ground Radar Objects. Boca Raton. doi: https://doi.org/10.1201/9781315214511

[14] Cole, J. B. (2002). High-accuracy Yee algorithm based on nonstandard finite differences: new developments and verifications. IEEE Transactions on Antennas and Propagation, 50 (9), 1185–1191. doi: https://doi.org/10.1109/tap.2002.801268

[15] Rylander, T., Bondeson, A. (2002). Application of stable FEM-FDTD hybrid to scattering problems. IEEE Transactions on Antennas and Propagation, 50 (2), 141–144. doi: https://doi.org/10.1109/8.997982

[16] Çakir, G. Çakir, M., Sevgi, L. (2008). Radar Cross Section (RCS) Modeling and Simulation, Part 2: A Novel FDTD-Based RCS Prediction Virtual Tool for the Resonance Regime. IEEE Antennas and Propagation Magazine. 50 (2), 81–94. doi: https://doi.org/10.1109/map.2008.4562259

[17] Volakis, J. L., Sertel, K. (2012). Integral Equation Methods for Electromagnetics. Institution of Engineering and Technology. doi: https://doi.org/10.1049/sbew045e

[18] Sukharevskiy, O. I., Zalevskiy, G. S., Nechitaylo, S. V., Sukharevskiy, I. O. (2010). Modelirovanie kharakteristik rasseyaniya vozdushnykh obektov rezonansnykh razmerov v metrovom diapazone voln. Izvestiya Vysshikh Uchebnykh Zavedeniy. Radioelektronika, 53 (4), 51–57. doi: https://doi.org/10.20535/s0021347010040060

[19] Yan, S., Jin, J.-M., Nie, Z. (2011). Improving the Accuracy of the Second-Kind Fredholm Integral Equations by Using the Buffa-Christiansen Functions. IEEE Transactions on Antennas and Propagation, 59 (4), 1299–1310. doi: https://doi.org/10.1109/tap.2011.2109364

[20] Zalevskiy, G. S., Vasilets, V. A., Sukharevskiy, O. I. (2014). Radar range profiles of cruise missiles in different wave bands. Applied Radio Electronics: Sci. Journ., 13 (1), 20–28. Available at: https://goo.su/UgP

[21] Ubeda, E., Tamayo, J. M., Rius, J. M. (2011). Taylor-orthogonal basis functions for the discretization in method of moments of second kind integral equations in the scattering analysis of perfectly conducting or dielectric objects. Progress In Electromagnetics Research, 119, 85–105. doi: https://doi.org/10.2528/pier11051715

[22] Yla-Oijala, P., Taskinen, M. (2005). Well-conditioned Muller formulation for electromagnetic scattering by dielectric objects. IEEE Transactions on Antennas and Propagation, 53 (10), 3316–3323. doi: https://doi.org/10.1109/tap.2005.856313

[23] Sukharevsky, O. I., Zalevsky, G. S., Vasilets, V. A. (2016). Modeling of Ultrawideband (UWB) Impulse Scattering by Aerial and Subsurface Resonant Objects Based on Integral Equation Solving. Advanced Ultrawideband Radar: Signals, Targets, and Applications. Chap. 5. Boca Raton, 195–235.

[24] Zalevsky, G. S., Sukharevsky, O. I., Vasylets, V. A. (2021). Integral equation modelling of unmanned aerial vehicle radar scattering characteristics in VHF to S frequency bands. IET Microwaves, Antennas & Propagation, 15 (10), 1299–1309. doi: https://doi.org/10.1049/mia2.12164

[25] Zalevsky, G., Brechka, M., Vasilets, V., Sukharevsky, O., Volkov, A., Horielyshev, S. (2020). Combined Calculation Method for the Scattering Characteristics of Complex Shaped Objects and Its Application to Model Helicopter Rotor Modulation Spectra. 2020 IEEE Ukrainian Microwave Week (UkrMW). doi: https://doi.org/10.1109/ukrmw49653.2020.9252754

[26] Zalevsky, G. S Sukharevsky, O. I. (2014). Calculation of scattering characteristics of aerial radar objects of resonant sizes based on iterative algorithm. Radioelectronics and Communications Systems, 57 (6), 244–253. doi: https://doi.org/10.3103/s0735272714060028

[27] Zalevsky, G. S., Muzychenko, A. V., Sukharevsky, O. I. (2012). Method of radar detection and identification of metal and dielectric objects with resonant sizes located in dielectric medium. Radioelectronics and Communications Systems, 55 (9), 393–404. doi: https://doi.org/10.3103/s0735272712090026

[28] Bakulev, P. A. (2004). Radiolokatsionnye sistemy. Moscow: Radiotekhnika, 320.

Received date 17.01.2022
Accepted date 11.06.2022
Published date 30.07.2022

How to cite: *Horielyshev, S., Volkov, P., Boikov, I., Baulin, D., Ivanets, H., Nakonechnyi, A., Manzhura, S., Yuriev, V., Gleizer, N. (2022). Study of the secondary characteristics of the bistatic scattering of a combined object in a covert radar surveillance system. EUREKA: Physics and Engineering, 4, 137–151. https://doi.org/10.21303/2461-4262.2022.002493*